Journal of Power Sources 193 (2009) 723–729

Contents lists available at ScienceDirect

Journal of Power Sources

journal homepage: www.elsevier.com/locate/jpowsour

Model-oriented cast ceramic tape seals for planar solid oxide fuel cells

Shaobai Sang[a,b], Jian Pu[a], Chi Bo[a], Li Jian[a,*]

[a] College of Materials Science and Engineering, State Key Laboratory of Material Processing and Die & Mould Technology, Huazhong University of Science and Technology, 1037 Luo Yu Lu, Wuhan, Hubei 430074, PR China
[b] State Key Laboratory Breeding Base of Refractories and Ceramics, Wuhan University of Science and Technology, Wuhan 430081, PR China

ARTICLE INFO

Article history:
Received 24 February 2009
Received in revised form 28 March 2009
Accepted 17 April 2009
Available online 3 May 2009

Keywords:
Ceramic tape seal
Capillary model
Alumina
Solid oxide fuel cell

ABSTRACT

A straight capillary model is developed to estimate the mass leak rate of the cast ceramic tape seals for planar solid oxide fuel cells (SOFCs), which is further rectified with consideration of microstructure complexity including the tortuosity, cross-section variation and cross-link of leak paths. The size distribution of the leak path, effective porosity and the microstructure complexity are the main factors that influence the leak rate of the cast tape seals. According to the model, Al_2O_3 powders are selected for preparation of the seals by tape casting, and the leak rate is evaluated under various compressive stresses and gauge pressures. The results indicate that Al_2O_3 powder with D_{50} value about 2 μm and specific surface area near 5 $m^2\ g^{-1}$ can be used for the cast tape seals; and the obtained leak rate can satisfy the allowable leak limit.

1. Introduction

In planar solid oxide fuel cells (SOFCs), sealing has been regarded as one of the most critical issues that limit the long-term operation of a SOFC stack. The seal material needs not only to be stable in the dual oxidizing and reducing environments but also to be electrically insulating and chemically compatible with other fuel cell components [1–3]. Conventional glass or glass-ceramic seals tend to transform in phases and react with cell components and interconnect materials under SOFC operating conditions in a long run, due to their intrinsic thermodynamical instability [4–6]. The deformable metallic seals, such as ductile silver [7,8] and corrugated or C-shaped super alloy gaskets [9], are limited by their high electronic conductivity. Although the hybrid mica-based seals have demonstrated excellent hermetic property, potassium element is still a potential concern for electrode poisoning.

In order to overcome the disadvantages presented in the aforementioned sealing materials, investigation of alternative sealing concepts has been the focus for years. Ceramic felts [10,11], ceramic papers [12] and cast ceramic tapes [13] with materials that are chemically stable in SOFC environments were reported as sealing components for planar SOFCs. The density of ceramic felts is usually low; pre-densification is needed before their applications. The cast ceramic tape seals are flexible and compressible to some extent; gapless contact can be maintained under moderate compressive stresses.

In the present study, flow mechanics modeling and experimental verification are carried out with cast Al_2O_3 tape seals. The purpose is to develop a physical model to estimate the leak rate of cast ceramic tape seals; accordingly, the factors that control the leak rate can be identified and analyzed and a preferred sealing microstructure can be suggested for achieving improved sealing property.

2. Model analysis

2.1. List of symbols

a	length of ceramic tape seal
b	thickness of ceramic tape seal
D	diameter of capillary or dimension of flow
D_0	expectation value of capillary diameter distribution
D_l	diameter of large capillary
D_s	diameter of small capillary
g	gravitational acceleration
Kn	Knudsen number
L	sealing width
L_e	actual length of leak path
l_l	length of large capillary
l_s	length of small capillary
$\dot{M}$	mass flow rate
$\dot{M}_{VD}$	mass flow rate in a capillary with variable diameters
$\dot{M}_{D_s}$	mass leak rate in a capillary with a constant diameter D_s
N	total number of capillary in tape seal
P	pressure

* Corresponding author. Tel.: +86 27 87557694; fax: +86 27 87558142.
E-mail address: lijian@hust.edu.cn (L. Jian).

0378-7753/$ – see front matter © 2009 Elsevier B.V. All rights reserved.
doi:10.1016/j.jpowsour.2009.04.032

P_i pressure inside SOFC stack
P_o pressure outside SOFC stack
Q total flow rate across a capillary
R radius of capillary
r radial distance
T temperature
t time
V gas velocity
V_s slip boundary velocity
α rarefaction coefficient
λ gas molecular free path
μ viscosity coefficient
ρ gas density
σ deviation of capillary diameter distribution
τ tortuosity
ϕ effective porosity of tape seal

Subscript
r component in radial coordinate direction
θ component in azimuth coordinate direction
x component in x coordinate direction
y component in y coordinate direction
z component in z coordinate direction

2.2. Modeling

At room temperature, the cast ceramic tape seal contains organic binder and additives, such as dispersant, plasticizer and lubricant, and can be placed in contact with the sealing surfaces perfectly with the aid of a small amount of solvent. At operating temperatures, the added organic binder and additives are burnt out, leaving interconnected pores in the tape seal. Therefore, it is considered that the leak through sealing interfaces is manageable, and the infiltration leak through the seal body is the primary concern in this model. Because the microstructure is complicated with various sizes and shapes of interconnected pores, it is difficult to define the boundary conditions of the leaking gas flow. Usually, the gas flow in such a microstructure can be idealized as that in a closed pipe network or a regular array of solid particles; however, a viable calculation of the leak rate remains problematical [14,15]. The approach used in the current model is to simplify the porous microstructure to straight capillaries with specific size distributions. The leak rate is calculated based on the simplified capillary structure, and then is corrected according to the realistic microstructure.

Three basic assumptions are made in the model: (1) all interconnected pores in the ceramic seal are visualized as straight capillaries lying in the direction of gas leak flow, and the diameter of the capillaries is in the range of 0.01–200 μm according to experimental observations and experiences; (2) in a ceramic seal with a length a, a thickness b and a sealing width L as shown in Fig. 1, the capillary diameter D obeys the Gaussian distribution:

$$f(D) = \frac{1}{\sqrt{2\pi}\sigma} e^{-(D-D_0)^2/2\sigma^2} \quad (1)$$

and (3) the probability for a diameter smaller than 200 μm must be greater than 99.8%, that is

$$P\{D < 200\} = \Phi\left(\frac{200 - D_0}{\sigma}\right) > 0.998 \quad (2)$$

where Φ is the standard function of normal distribution.

2.3. Calculation of mass flow rate

H_2 is chosen as the gas of investigation. H_2 leaks through the capillaries under the condition that the pressure inside the SOFC stack P_i is higher than that outside P_o. Similar to the case of interface leak in mica-based seals [16], the flow characteristics of the high-temperature gas should be considered, as the gas flow is confined in such micro-channels. The average molecular free path of H_2 gas is 0.60 μm at 750 °C which is the operating temperature of the planar SOFC studied. The pressure-driven leak flow can be considered to be a continuum laminar flow in capillaries with diameters in the range of 60–200 μm; and the flow falls into the slip or transition flow regime if the diameter of the capillary is smaller than 60 μm, according to the value of the Knudsen number ($Kn = \lambda/D$, defined as the degree of gas rarefaction). In subsequent sections, these two situations are considered individually:

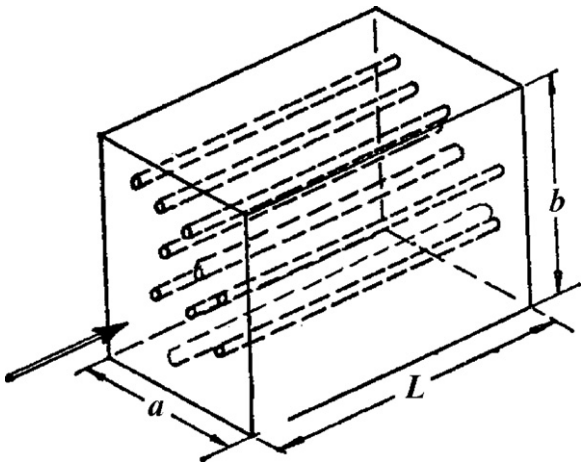

Fig. 1. Schematic drawing of the simplified porous microstructure in which capillaries with various diameters lying in leak flow direction represents interconnected pores. The diameter of the capillaries obeys the Gaussian distribution.

(1) Laminar flow in capillaries with $60 \le D \le 200$ μm.
Fig. 2 shows a capillary referenced in both cylindrical and Cartesian coordinates. The pressure-driven H_2 leak flow is regarded as a continuum laminar flow that can be described by the Navier–Stokes equations:

$$\begin{cases} \dfrac{\partial V_r}{\partial t} + (V\cdot\nabla)V_r - \dfrac{V_\theta^2}{r} = g_x - \dfrac{1}{\rho}\dfrac{\partial P}{\partial r} + \nu\left(\nabla^2 V_r - \dfrac{2}{r^2}\dfrac{\partial V_\theta}{\partial \theta} - \dfrac{V_r}{r^2}\right) \\ \dfrac{\partial V_\theta}{\partial t} + (V\cdot\nabla)V_\theta - \dfrac{V_r V_\theta}{r} = g_\theta - \dfrac{1}{\rho r}\dfrac{\partial P}{\partial \theta} + \nu\left(\nabla^2 V_\theta + \dfrac{2}{r^2}\dfrac{\partial V_r}{\partial \theta} - \dfrac{V_\theta}{r^2}\right) \\ \dfrac{\partial V_z}{\partial t} + (V\cdot\nabla)V_z = g_z - \dfrac{1}{\rho}\dfrac{\partial P}{\partial z} + \nu\nabla^2 V_z \end{cases} \quad (3)$$

where ν is defined as μ/ρ. Considering the leak flow of H_2 in a planar SOFC stack, it is further assumed that:
(i) the flow is isothermal and steady;
(ii) H_2 gas is incompressible, and the gravity effect of H_2 is ignored, $g_x = g_\theta = g_z = 0$;
(iii) the velocity slip is neglected and the flow velocity at the capillary wall is zero.

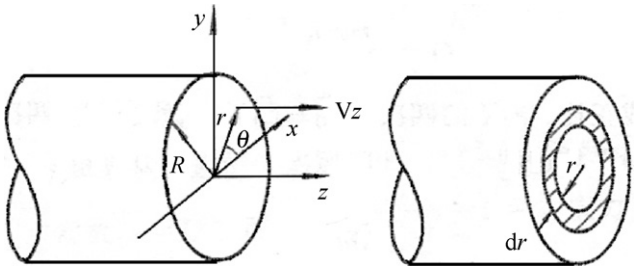

Fig. 2. Cylindrical and Cartesian coordinates showing the capillary model of the lamellar flow.

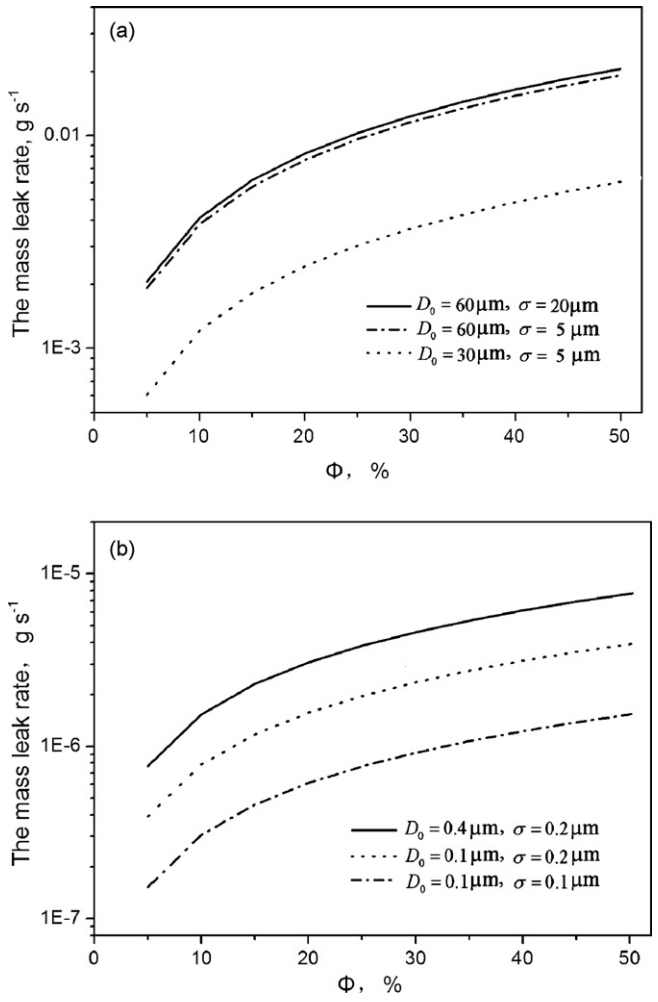

Fig. 3. Mass leak rate of H_2 calculated from the developed model with various Gaussian distributions of the capillary diameter.

The gas flow direction parallels with z-axis, and the velocity components in the x- and y-directions equal to zero. Further assuming that the pressure difference in the direction of capillary length L is

$$-\frac{\partial P}{\partial x} = \frac{\Delta P}{L}$$

the total flow rate of a capillary Q as a function of its radius R can be obtained by solving the Navier–Stokes equations [18]:

$$Q = \frac{\pi R^4 \Delta P}{8\mu L} \tag{4}$$

(2) Slip and transition flows in capillaries with $0.01 \le D < 60$ μm.

As mentioned above, for capillaries with diameters in the range of 0.01–60 μm, the flow is categorized as the slip or transition flow for which the conventionally assumed no-slip boundary condition is no longer applicable, a Knudsen layer with a thickness in the order of molecular free path plays a decisive role. Furthermore, as the capillary diameter decreased, collisions between gas molecules and capillary walls are required to be taken into account; and the kinematic viscosity of momentum diffusion should be modified for the enhanced rarefaction effect. Thus an unified flow model for both the slip and transition flows is established, in which the flow in a capillary is divided into two layers, i.e. the Knudsen layer and the middle layer, with a continuous transition in between. The enhanced

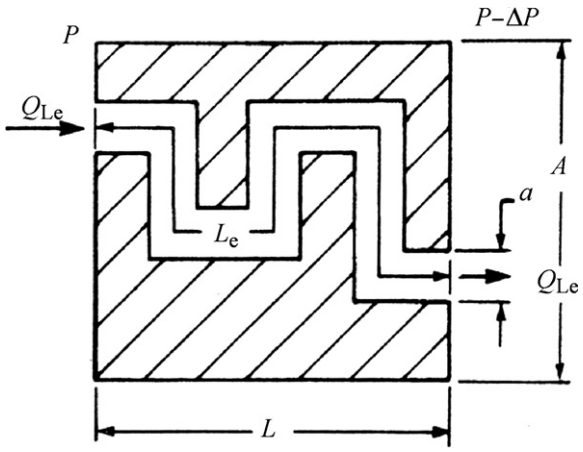

Fig. 4. Schematic presentation of physical definition of the tortuosity.

rarefaction effect is considered by introducing the rarefaction coefficient $C_r(Kn)$ that is a function of Kn. For the pressure-driven incompressible flow in such a capillary, the velocity slip boundary condition is

$$V_s = \frac{R^2}{4\mu} \cdot \frac{\partial P}{\partial z} \cdot \frac{3Kn + 1}{Kn + 1} \tag{5}$$

In addition to the assumptions made in the laminar flow mode, it is further assumed that:

(i) temperature gradient inside the leak flow is neglected, even though temperature fluctuation is more likely to happen in the slip and transition flows;

(ii) the rarefaction coefficient $C_r(Kn)$ is given as [17].

$$C_r(Kn) = 1 + \alpha Kn \tag{6}$$

where

$$\alpha = 1.358 \frac{2}{\pi} \tan^{-1}(4Kn^{0.4})$$

Applying the above assumptions and the velocity slip boundary condition (Eq. (5)), the flow rate of a capillary with $0.01 \le D < 60$ μm can be derived as [18]:

$$Q = \frac{\pi R^4 \Delta P}{8\mu L}[1 + 0.865 \tan^{-1}(4Kn^{0.4})]\left(1 + \frac{4Kn}{1 + Kn}\right) \tag{7}$$

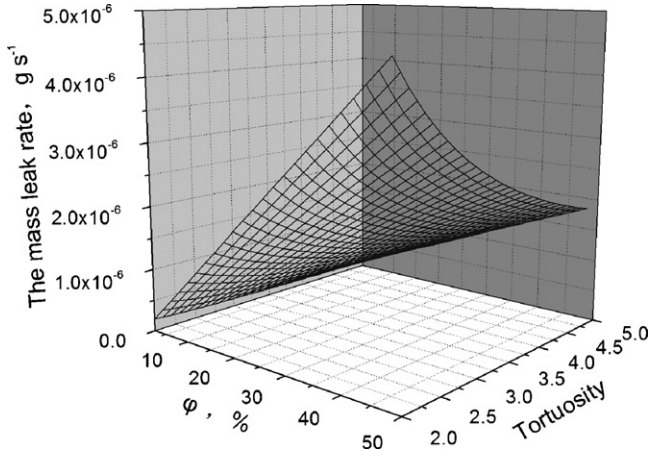

Fig. 5. Calculated mass leak rate of H_2 as a function of the effective porosity and tortuosity with $D_0 = 0.4$ μm and $\sigma = 0.2$ μm.

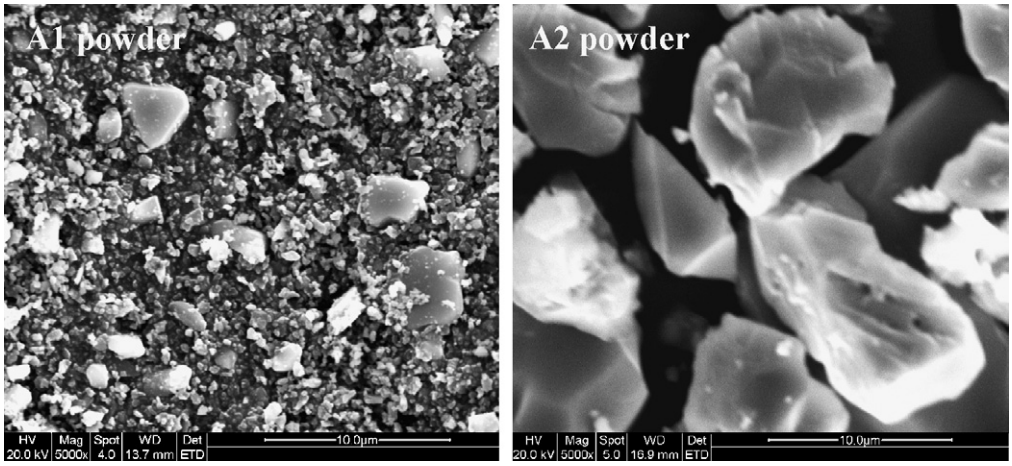

Fig. 6. SEM micrographs of Al_2O_3 powders used for preparing the cast tape seals.

The leak rate of the cast ceramic tape seal can be obtained theoretically by summation of the leak rate in each capillary, provided the quantity of the capillary is available. Assuming that there are N capillaries in a tape seal and the diameter scale is divided into i intervals between the minimum and maximum diameters as $(D_{\min}, D_1), (D_1, D_2), (D_2, D_3), \ldots, (D_{i-2}, D_{i-1}), (D_{i-1}, D_{\max})$, then the number of capillary with diameters in the range of (D_k, D_{k+1}), n_k, can be expressed as:

$$n_k = N \cdot \int_{D_k}^{D_k+\Delta D_k} \frac{1}{\sqrt{2\pi}\sigma} e^{-(D-D_0)^2/2\sigma^2} dD \tag{8}$$

where $\Delta D_k = D_{k+1} - D_k$, $k = 1, 2, 3, \ldots, i$. Defining the effective porosity of the tape seal ϕ as the volume ratio of all capillaries to the seal, ϕ can be approximately expressed as a function of capillary diameter and quantity as follow as long as ΔD_k is infinitesimal:

$$\begin{aligned}\phi &= \frac{1}{ab}\left[\frac{\pi D_{\min}^2}{4}\cdot n_1 + \frac{\pi D_1^2}{4}\cdot n_2 + \cdots + \frac{\pi D_{i-2}^2}{4}\cdot n_{i-2} + \frac{\pi D_{i-2}^2}{4}\cdot n_{i-1}\right] \\ &= \frac{N}{ab}\cdot\left[\frac{\pi D_{\min}^2}{4}\int_{D_{\min}}^{D_1}\frac{1}{\sqrt{2\pi}\sigma}e^{-(D-D_0)^2/2\sigma^2}dD\right. \\ &+ \frac{\pi D_1^2}{4}\int_{D_1}^{D_2}\frac{1}{\sqrt{2\pi}\sigma}e^{-(D-D_0)^2/2\sigma^2}dD + \cdots \\ &+ \frac{\pi D_{i-2}^2}{4}\int_{D_{i-2}}^{D_{i-1}}\frac{1}{\sqrt{2\pi}\sigma}e^{-(D-D_0)^2/2\sigma^2}dD \\ &+ \left.\frac{\pi D_{i-1}^2}{4}\int_{D_{i-1}}^{D_{\max}}\frac{1}{\sqrt{2\pi}\sigma}e^{-(D-D_0)^2/2\sigma^2}dD\right]\end{aligned} \tag{9}$$

With given ϕ and $f(D)$, N can be determined using Eq. (9). The ϕ can be normally measured by mercury intrusion porosimetry in the form of cumulative volume penetrated per mass of specimen as a function of pore radius, from which the fractional pore (capillary) size distribution $f(D)$ can be derived.

For capillaries with diameters between 60 and 200 μm, the contribution of the capillaries within the interval (D_k, D_{k+1}) to the mass flow rate is

$$\begin{aligned}\dot{M}_k &= \rho \cdot n_k \cdot \frac{\pi\ \Delta P D_k^4}{128\mu L} \\ &= \frac{2P_o}{RT}\cdot N \cdot \int_{D_k}^{D_{k+1}}\frac{1}{\sqrt{2\pi}\sigma}e^{-(D-D_0)^2/2\sigma^2}dD \cdot \frac{\pi\ \Delta P D_k^4}{128\mu L} \\ &= N \cdot \frac{\pi P_o\ \Delta P D_k^4}{64\mu RTL}\cdot\int_{D_k}^{D_{k+1}}\frac{1}{\sqrt{2\pi}\sigma}e^{-(D-D_0)^2/2\sigma^2}dD\end{aligned} \tag{10}$$

If the interval (D_k, D_{k+1}) falls into to the range of 0.1–60 μm, then:

$$\begin{aligned}\dot{M}_k &= \rho \cdot n_k \cdot \frac{\pi\ \Delta P D_k^4}{128\mu L}[1 + 0.865\ \tan^{-1}(4Kn^{0.4})]\left(1 + \frac{4Kn}{1+Kn}\right) \\ &= N \cdot \frac{\pi P_o\ \Delta P {D_k}^4}{64\mu RTL}[1 + 0.865\ \tan^{-1}(4Kn^{0.4})] \\ &\times \left(1 + \frac{4Kn}{1+Kn}\right)\cdot\int_{D_k}^{D_{k+1}}\frac{1}{\sqrt{2\pi}\sigma}e^{-(D-D_0)^2/2\sigma^2}dD\end{aligned} \tag{11}$$

For a tape seal with width a and thickness b, the total mass leak rate can be calculated by the summation of $\dot{M}_k$:

$$\dot{M} = \sum_{k=1}^{i-1}\dot{M}_k \tag{12}$$

It can be seen that both the effective porosity ϕ and the size distribution of the capillary affect the mass leak rate. According to the calculation results, as shown in Fig. 3, with $a = 1$ cm, $b = 0.5$ μm, $L = 1$ cm, $P_i = 1.048 \times 10^5$ Pa, $P_o = 1.013 \times 10^5$ Pa, $\mu = 1.92 \times 10^{-7}$ Pa s and $T = 750\,^\circ$C, the mass leak rate increases significantly as D_0 increases in the range above tens of microns; σ presents more meaningful effect than that of D_0 while D_0 is in the range of submicrons. It is further known from the results that it is possible to achieve effective sealing by reducing the pore size in the seal, even though the porosity of the seal is reasonably large. For example, with capillary diameters in the range of 0.01–0.5 μm (D_0 is 0.1 μm

Table 1
The providers and specification of Al_2O_3 powders used for preparing the tape seals.

Type	Provider	D_{10} (μm)	D_{50} (μm)	D_{90} (μm)	Specific surface area ($m^2\ g^{-1}$)
A1	Almatis Inc.	0.3	1.90	4.19	5.40
A2	Tian Ma Micro Powders	10.11	15.46	25.22	1.09

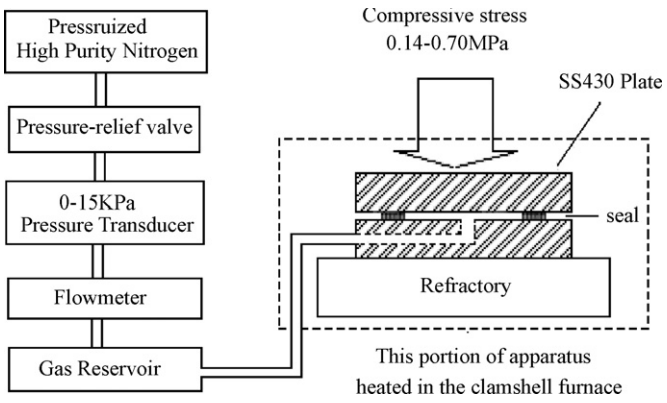

Fig. 7. Schematic of the in-house set-up for leak test.

and σ is 0.1 μm), the mass leak rate is 6×10^{-7} g s^{-1} for a ϕ of 20% used in the calculation, as shown in Fig. 3(b). Therefore, it can be predicted that relatively large pores must be avoided and uniform fine pores are allowed in the cast ceramic tape seals for obtaining robust sealing effect.

2.4. Model rectification

2.4.1. Tortuosity of leak path

The real leak path in cast ceramic tape seals is squiggly, characterized by the term tortuosity τ defined as:

$$\tau = \left(\frac{L_e}{L}\right)^2$$

and schematically shown in Fig. 4. In this case, the capillary quantity in the seal reduces to L/L_e of that in the straight capillary model if the effective porosity remains unchanged; and so does the flow rate in each capillary if the gas pressure difference maintains the same. Combining the above two factors, the total mass leak rate decreases to $1/\tau$ of that as predicted in the straight capillary model. The value of τ was reported between 2.0 and 2.5 [14]; and the corrected leak rate by the tortuosity will be at least less than 1/2 of that obtained from the model. Fig. 5 shows an example calculation of the mass leak rate of H_2 with a D_0 of 0.4 μm and a σ of 0.2 μm and variations of ϕ and τ. The mass leak rate decreases significantly with increased leak path tortuosity.

2.4.2. Cross-section variation of leak path

In the capillary model, it is assumed implicitly that the diameter of each single capillary is the same along its length; however, the cross-section of actual leak paths in ceramic tape seals is variable. The mass flow rate in a capillary with a variable diameter will be smaller than that with a fixed diameter. In the case of a straight capillary with two different diameters D_l and D_s and corresponding capillary lengths l_l and l_s, the mass flow rate in this variable diameter capillary $\dot{M}_{VD}$ can be expressed as:

$$\dot{M}_{VD} = \dot{M}_{D_s} \frac{x^4(1+y)}{(x^4+y)} \frac{(1+yx)^2}{(1+yx^2)^3} \quad (13)$$

where $x = D_l/D_s$ and $y = l_l/l_s$, according to the Hagen–Poiseuille equations without considering the flow loss caused by diameter sharp change at the connection. It can be proved that $\dot{M}_{VD}$ is always smaller than $\dot{M}_{D_s}$ as long as the diameter changes. For instance, $\dot{M}_{VD} = 0.27\dot{M}_{D_s}$ for $x = 2$ and $y = 1$.

2.4.3. Cross-link of leak path

Leak paths in ceramic tape seals are likely to form interconnected network structure if the porosity of the seal is larger than 10%. A three-dimensional capillary model [19] assumed that $N/3$ capillaries parallel to each of the x-, y- and z-axes, respectively, and the total leak rate in the flow direction is 1/3 of that predicted by the model with N capillaries lying in the flow direction. In the present model, one-dimensional leak along the sealing width is

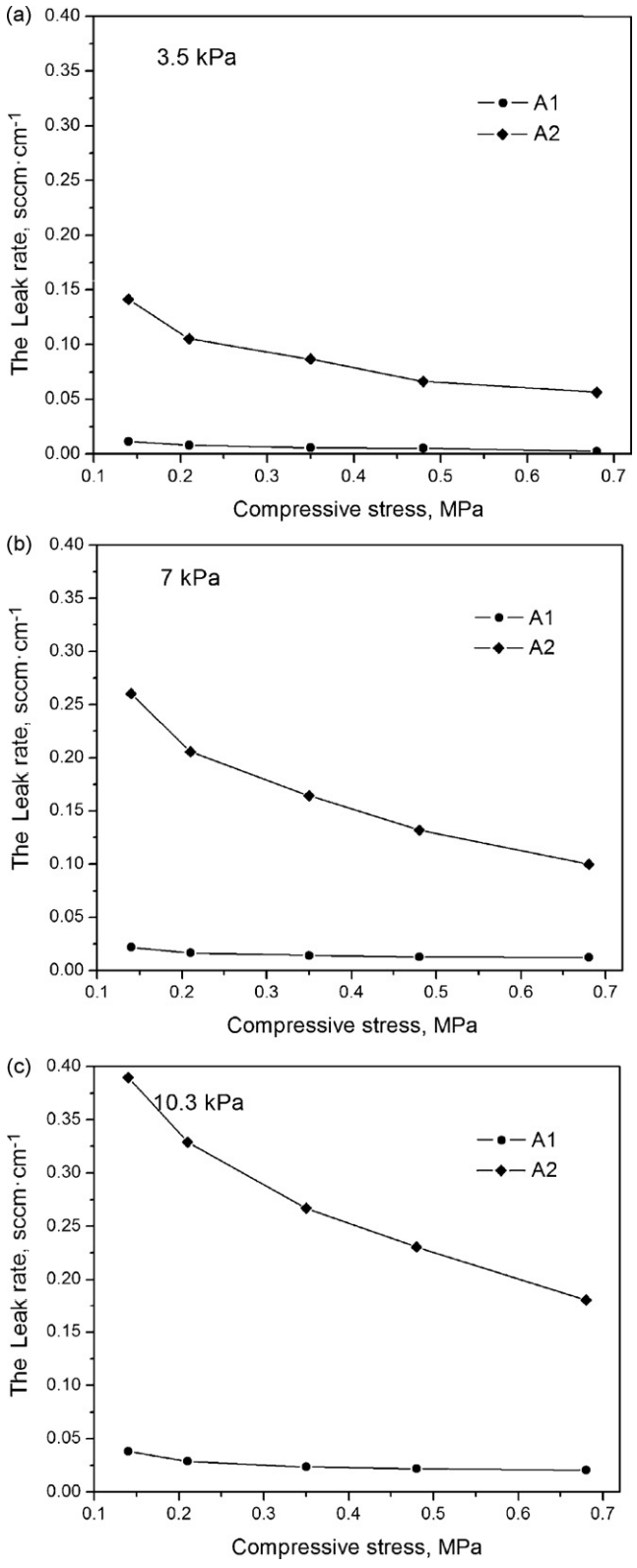

Fig. 8. Leak rates of the A1 and A2 cast tape seals at different compressive stresses and gas pressures.

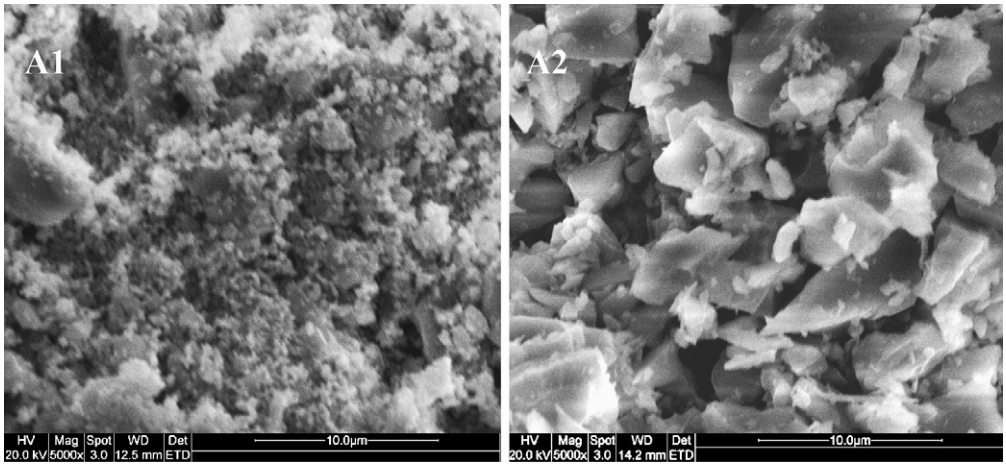

Fig. 9. Post-test microstructures of the A1 and A2 tape seals under compressive stress of 0.14 MPa.

assumed; therefore, with the correction of leak path cross-link, the actual mass flow rate will be 1/3 of that predicted by the one-dimensional capillary model as long as the effective porosity remains unchanged.

Based on the model analysis, it is understood that the pore size distribution, the porosity, and the complexity of leak paths (tortuosity, cross-section variation and cross-link) are the main factors that determine the mass leak rate of the ceramic tape seals. In order to achieve robust sealing performance in planar SOFCs with the cast tape seals, the microstructure of the tape seals is required to be controlled by design so as to obtain fine pores with variable size, low porosity and high tortuosity.

3. Design of cast ceramic tape seals for planar SOFCs

For a $10\,cm \times 10\,cm$ planar cell with an active area of $9\,cm \times 9\,cm = 81\,cm^2$, the sealing component is a window frame with an outer sealing length of $4 \times 10\,cm = 40\,cm$ per cell. Assuming the cell is operated under current density of $0.7\,A\,cm^{-2}$, $5.88 \times 10^{-4}\,g\,s^{-1}$ of pure H_2 are needed theoretically. The H_2 usage becomes to $7.35 \times 10^{-4}\,g\,s^{-1}$ if 80% fuel utilization is considered. Taking 0.5% of the total flow as the allowable H_2 leak up-limit for safety concern, the mass leak rate must be lower than $9.22 \times 10^{-8}\,g\,s^{-1}\,cm^{-1}$, that is $0.06\,sccm\,cm^{-1}$. In order to fulfill this rigorous criterion, the main factors influencing gas leak rate in the cast ceramic tape seal, as discussed above, must be carefully controlled by design.

Considering the effect of tortuosity (factor of ~1/4), cross-section variation (factor of ~1/3) and cross-link (factor of ~1/3) of leak paths, the mass leak rate of the ceramic tape seal is reasonably assumed to be at least one order of magnitude lower than that predicted by the straight capillary model, thus the leak up-limit $9.22 \times 10^{-7}\,g\,s^{-1}\,cm^{-1}$ is used for selecting the microstructure parameters according to the straight capillary model. It can be seen from Fig. 3(b) that submicron leak paths and significantly low effective porosity are required for obtaining a leak rate as low as $9.22 \times 10^{-7}\,g\,s^{-1}\,cm^{-1}$.

In the cast ceramic tape seal, the pore size and porosity are basically determined by the packing of ceramic particles, the shape and size distribution of the particles are of importance for achieving fine pore size and low porosity to satisfy the low leak rate requirement. For equally sized spherical particles, the densest packing mode is the face-centered-cubic or close-packed hexagonal stacking with a porosity of 26%. And the porosity can be further reduced to much lower than 22%, provided the pores in the close-packing of spherical particles are filled by even smaller particles. Following this design consideration, the pore size or the size of leak paths can be decreased into the region of submicrons by using sphere-like ceramic powders with particle size distributed from several microns to submicrons for fabrication of the tape seal. Thus the requirement of mass leak rate below $9.22 \times 10^{-8}\,g\,s^{-1}\,cm^{-1}$ can be met. According to the above design, cast ceramic tape seals were prepared and evaluated to verify the effectiveness of the model.

4. Preparation and verification of the cast ceramic seals

Two different Al_2O_3 powders, A1 and A2 as listed in Table 1, were selected as raw materials for preparing the cast tape seals. A1 is a fine Al_2O_3 powder with an average particle size smaller than 5 μm, and the particle size of the A2 is relatively coarse with an average particle size in the range of tens of microns. Fig. 6 shows the scanning electron microscope (SEM, QUANTA 200, FEI) images of the two powders.

The Al_2O_3 seals were prepared by tape casting with organic solvent, binder, dispersant and plasticizers as described in detail in Ref. [13]. The thickness of the dried tape seals was around 0.40 mm and no surface defects were observed. The cast tape seals were flexible at room temperature, and could be placed in close contact with the sealing surfaces under a moderate compressive force. Window frame samples were formed with an outside dimension of $7\,cm \times 7\,cm$ and an inside dimension of $5\,cm \times 5\,cm$ for the leak test by using an in-house designed set-up as shown in Fig. 7 [13]. The test gas used was N_2, the obtained leak rate was converted to that of H_2 by changing the parameters μ and Kn. The window frame specimen was placed in between two polished stainless steel plates under a compressive load, and heated in a clamshell furnace at a heating rate of $1\,^{\circ}C\,min^{-1}$ to 200 °C, and dwelled for 90 min followed by further heating at $2\,^{\circ}C\,min^{-1}$ up to 750 °C. The gas leakage from the seal was read from a rotometer (FL-310, OMGEA Engineering Inc., USA) after the equilibrium was reached. The leak rate was obtained by dividing the rotometer reading with the inside perimeter of the window frame sample. The compressive stress was varied from 0.14 to 0.69 MPa and the applied gauge pressure was 3.5, 6.9 or 10.3 kPa, respectively.

Fig. 8 shows the leak rates of the cast tape seals made from A1 and A2 powders under various compressive stresses and gas pressures. The leak rate of A1 tape seals is below $0.04\,sccm\,cm^{-1}$ in all cases, and lowered with increasing the compressive stress and decreasing the gauge pressure. However, the leak rate of A2 seals is much higher than that of A1 seals under various conditions. The function of the compressive stress is to maintain a good contact between the seal and the sealing surfaces to minimize the interface

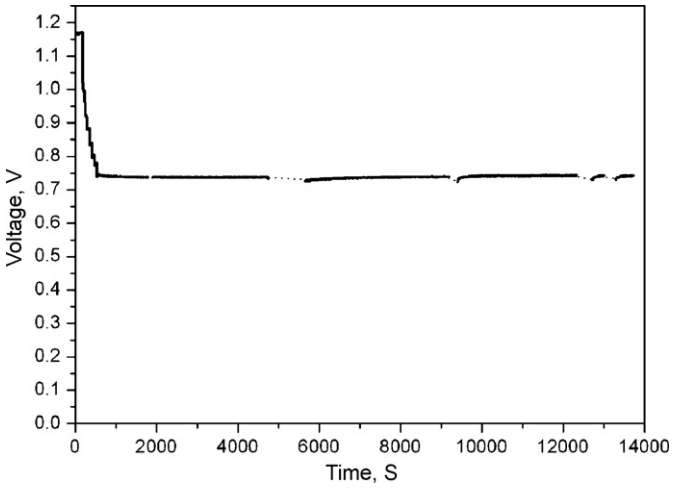

Fig. 10. SOFC single cell performance under a current density of 500 mA cm^{-2} with the A1 seal.

leak and a higher packing density of the tape seal. Fig. 9 shows the microstructure of post-test Al_2O_3 seals tested at a compressive stress of 0.14 MPa. A1 seal is densely packed with pores smaller than 0.5 μm; in contrast, A2 seal is relatively loosely packed with pores bigger than 2 μm. These results suggest that A1 seals can meet the requirement on the mass leak rate as predicted by the model and A2 seals cannot be considered in SOFC applications.

In order to further verify the applicability of A1 seal in real planar SOFCs, a single cell test was conducted at 750 °C with the A1 as the seal. A high open circuit voltage of 1.17 V and a steady performance under a current density of 500 mA cm^{-2} were achieved, as shown in Fig. 10.

5. Conclusion

Based on the model study and experimental verification, the following conclusions are made:

(1) The leak rate of cast ceramic tape seals can be approximately estimated by the developed capillary model corrected with considerations of tortuosity, cross-section variation and cross-link of the leak paths.
(2) The main factors influencing the leak rate of the cast ceramic tape seals are leak path size distribution, effective porosity and microstructure complexity (tortuosity, cross-variation and cross-link of leak paths).
(3) Sphere-like ceramic powders with an average particle size of several microns and a relatively wide size distribution are preferred for the cast tape seals.
(4) The leak rate of Al_2O_3 tape seals is lowered under increased compressive stress and decreased gauge pressure. Fine Al_2O_3 powders with D_{50} value about 2 μm and specific surface area near 5 $m^2\,g^{-1}$ can be used for the cast tape seals; and the leak rate can satisfy the requirement of planar SOFC applications.

Acknowledgements

This project is financially supported by the Ministry of Science and Technology of China under the national “863” project 2006AA05Z148, by the City of Wuhan under the key project 200710321087 and by the State Key Laboratory of Material Processing and Die & Mould Technology. The SEM examination was assisted by the Analytic and Testing Center of Huazhong University of Science and Technology.

References

[1] R.N. Singh, Ceram. Eng. Sci. Proc. 25 (3) (2004) 299–307.
[2] W.F. Jeffrey, J. Power Sources 147 (2005) 46–57.
[3] C.A. Lewinsohn, S. Elangovan, S.M. Quist, Ceram. Eng. Sci. Proc. 25 (3) (2004) 315–320.
[4] L. Peng, Q.S. Zhu, C.H. Xie, et al., J. Inorg. Mater. (Chin.) 21 (4) (2006) 867–872.
[5] S.P. Jiang, L. Christiansen, B. Hughan, K. Foger, J. Mater. Sci. Lett. 20 (8) (2001) 695–697.
[6] Z. Yang, J.W. Stevenson, K.D. Meinhardt, Solid State Ionics 160 (2003) 213–225.
[7] J. Duquette, A. Petric, J. Power Sources 137 (1) (2004) 71–75.
[8] Y.S. Chou, J.W. Stevenson, J. Mater. Res. 18 (9) (2003) 2243–2250.
[9] K.S. Weil, J.S. Hardy, Ceram. Eng. Sci. Proc. 25 (3) (2004) 321–326.
[10] D. Ghosh, R. Wang, E. Brule, P. Tang, in: S. Singhal, M. Dokiya (Eds.), Electrochemical Society Proceedings, 1999, pp. 822–829.
[11] D. Ghosh, M.E. Pastula, R. Boersma, D. Prediger, M. Perry, A. Hovath, J. Devitt, Proceedings of the Fuel Cell Seminar, Washington, DC, 2000, pp. 511–514.
[12] B. Martin, R. Stephan, D. Pere, et al., J. Power Sources (2004) 138111–138119.
[13] S. Sang, W. Li, J. Pu, et al., J. Power Sources 177 (2008) 77–82.
[14] X.Y. Kong, Advanced Mechanics of Fluids in Porous Media, China Science & Technology University Press, Hefei, 1999, P21–P22.
[15] J. Bear, in: J.S. Li, C.X. Chen (Eds.), Kinetics of Fluids in Porous Media, China Architecture & Building Press, Beijing, 1983.
[16] S. Sang, J. Pu, S. Jiang, L. Jian, J. Power Sources 182 (2008) 141–144.
[17] G.E. Karniadakis, A. Beskok (Eds.), Micro Flow Fundamentals and Simulation, Springer-Verlag, New York, 2002.
[18] S. Shaobai, Design and performance optimization of seals for solid oxide fuel cells, Ph.D. Thesis, Huazhong University of Science and Technology, 2008.
[19] F.A.L. Dullien, Porous media: fluid transport and pore structure, Translated by Y.P. Fan, D.W. Zhao, Xian Dai Shen Liu Wu Li Xue, Petroleum Industry Press, Beijing, 2001.